Received: 7 November 2023 | Revised: 22 January 2024 | Accepted: 20 February 2024

DOI: 10.1002/nag.3720

RESEARCH ARTICLE

WILEY

Interpreting correlations in stress-dependent permeability, porosity, and compressibility of rocks: A viewpoint from finite strain theory

Luyu Wang[1] | **Yanjun Zhang**[2]

[1]Department of Civil and Environmental Engineering, The Hong Kong Polytechnic University, Hung Hom, Kowloon, Hong Kong SAR, China

[2]College of Petroleum Engineering, Xi'an Shiyou University, Xi'an, Shaanxi, China

Correspondence
Luyu Wang, Department of Civil and Environmental Engineering, The Hong Kong Polytechnic University, Hung Hom, Kowloon, Hong Kong SAR, China.
Email: luyu.wang@polyu.edu.hk

Yanjun Zhang, College of Petroleum Engineering, Xi'an Shiyou University, Xi'an 710065, China.
Email: yanjun21@xsyu.edu.cn

Funding information
National Natural Science Foundation of China, Grant/Award Number: 52304039

Abstract

Characteristics of stress-dependent properties of rocks are commonly described by empirical laws. It is crucial to establish a universal law that connects rock properties with stress. The present study focuses on exploring the correlations among permeability, porosity, and compressibility observed in experiments. To achieve this, we propose a novel finite strain-based dual-component (FS-DC) model, grounded in the finite strain theory within the framework of continuum mechanics. The FS-DC model decomposes the original problem into the rock matrix and micro-pores/cracks components. The deformation gradient tensor is utilized to derive the constitutive relations. One of the novelties is that the stress-dependent variables are calculated in the current configuration, in contrast to the reference configuration used in small deformation theory. The model has only a few number of parameters, each with specific physical interpretations. It can be reduced to existing models with appropriate simplifications. Then, model performance is examined against experimental data, including permeability, porosity, compressibility, volumetric strain and specific storage. It proves that the variations of these properties are effectively described by the proposed model. Further analysis reveals the effect of pores/cracks parameters. The validity of the FS-DC model is examined across a broad range of pressures. The results show that rock properties at high confining pressures (>300 MPa) differ from those observed under relatively low pressures (<200 MPa). This disparity can be attributed to inelastic behaviors of micro-structure, wherein the rock skeleton undergoes permanent deformation and breakage.

KEYWORDS
finite strain theory, large deformation, permeability, petrophysics, porosity, rock compaction

1 | INTRODUCTION

1.1 | Stress-dependent properties of rock

Investigating stress-dependent properties of rock plays a pivotal role in understanding the mechanisms underlying geomechanical processes, including hydrology, geophysics, and reservoir engineering.[1–3] Exploring the correlations among permeability, porosity, and compressibility under varying stresses provides insights into unraveling the mechanisms behind these processes.[4–6]

Experiments and analytical models have been developed to analyze the mechanisms governing the evolution of rock properties in response to varying stresses. The experiments involve subjecting rock specimens to diverse confining stresses and pore pressures, replicating the stress conditions in underground environment,[7–10] allowing for the measurement of rock properties such as permeability, porosity, and compressibility.[11–14] Existing models are either empirically established based on experimental results or theoretically derived using small deformation theory.[15–19] While these existing methods have gained successes in applications, it is still imperative to develop a unified law for describing the characteristics of stress-dependent properties.[20–22]

Notably, Zimmerman[23] discussed the applicability of finite strain theory in rock deformation analysis, and pointed out that the accuracy of the small deformation theory is acceptable for most geophysical problems. However, in extreme environments, characterized by very high confining pressures, rocks may exhibit different properties compared to conditions with relatively low pressure levels.[9,10] The conventional small deformation formulation may be inadequate to capture such properties.

1.2 | The necessity of introducing finite strain theory

1.2.1 | Experimental evidences

Many experimental results indicate that rocks undergo large deformation in certain scenarios. The reasons can be summarized in two aspects: (1) high confining pressure, and (2) rocks with high porosity. As a case in point, David et al.[9] observed that the porosity of sandstone, such as Boise sandstone (with porosity 35% in unstressed state), significantly decreases under high confining pressure (300∼500 MPa), and the reduction in porosity can reach up to 15%∼20%. Moreover, Dong et al.[10] reported a reduction of 10%∼20% in the porosity of fine-grained sandstone and shale as the confining pressure increased within the range of 3∼120 MPa. Additionally, many authors have conducted experiments focusing on stress-induced variations in rock properties.[11,13,20,21,23–25] A more detailed analysis of the experimental results will be provided in Sections 6 in this article.

Experimental results suggest a nonlinear relation between variations of stress and strain, which can be attributed to the heterogeneous nature of rocks. This phenomenon may be explained by the reduction in porosity, leading to the closure of pores and cracks that undergo large deformation (finite strain).[26,27] Therefore, it is necessary to introduce the finite strain theory, which demonstrates superior performance compared to the conventional small deformation theory.

1.2.2 | Limitations of the small deformation theory

The conventional small deformation theory may be inadequate for accurately characterizing rock compression, given the limited information available within the current configuration of a deformed rock specimen.[28,29] The term "current configuration" is defined within the framework of finite strain theory in continuum mechanics.[30,31] In contrast, the small deformation theory utilizes a strain measurement attached to the "reference configuration", which is a concept opposite to the current configuration.

To clarify the difference between these two formulations, Figure 1 shows the deformation of a porous rock in reference and current configurations. The accuracy of strain may be compromised if one insists on using the strain defined in the reference configuration. A more accurate alternative is the finite strain, defined in the current configuration. Some authors have attempted to utilize the real strain, which stands in contrast to the engineering strain. For instance, Liu et al.[28] pioneered the two-part Hooke's model incorporating the real strain, and this model has been refined by numerous researchers in enhanced versions.[29,32,33]

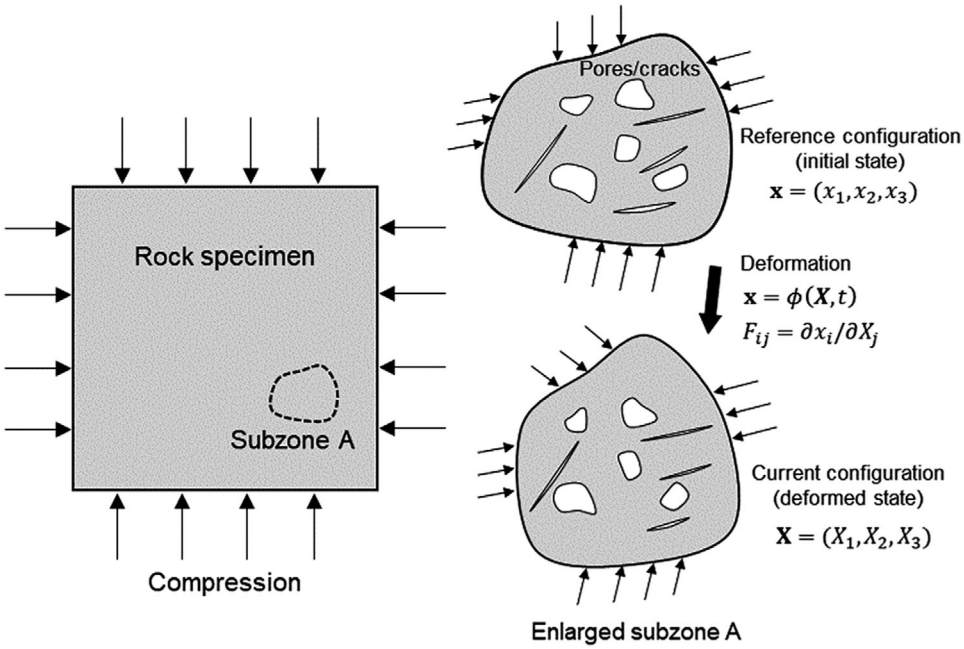

FIGURE 1 Conceptual schematic of the reference and current configurations in rock deformation.

However, the existing models[15–17,19,21,22] lack a foundation in the finite strain framework, and the stress-dependent porosity is defined with the respect to the reference configuration rather than the current configuration. This treatment may induce inaccuracies, particularly under conditions with high confining pressure and closure of micro-cracks. Moreover, in these models, parameters lack physical significance, and the procedure for determining parameters is complicated.[28,29] To address the limitations, in this study, we develop a dual-component model with the finite strain theory within the framework of continuum mechanics.

1.3 | Aim of this study

In this study, we aim to develop a finite strain-based model that provides theoretical interpretations for the correlations among stress-dependent properties of rocks. The article is organized as follows. First, the finite strain-based dual-component (FS-DC) model is proposed in Section 2. In Section 3, the stress-dependent quantities are determined based on the finite strain formulation. The procedure for determining model parameters is given in Section 4. The data source is provided in Section 5. Then, in Section 6, we employ the proposed FS-DC model to analyze experimental results from various rock types. The effects of pores/cracks and rock bulk properties are explored. A comprehensive analysis is performed to assess the applicability of the model across a broad range of pressures.

2 | FORMULATION OF DUAL-COMPONENT MODEL WITH FINITE STRAIN

In this section, we establish the dual-component model, which conceptualizes the original problem as a combination of the rock matrix and micro-pores/cracks parts. Rock strains are calculated in the current configuration, where the volumetric strain is derived through a finite strain formulation that involves the deformation gradient tensor.

2.1 | The dual-component model

The dual-component model is established based on the observation that the pores and cracks and the rock matrix each make distinct contributions to the overall deformation of rock. Experimental results prove that under low confining pressure conditions, pores and cracks initially close, followed by the deformation of the rock matrix as the confining pressure increases.[9,10,13]

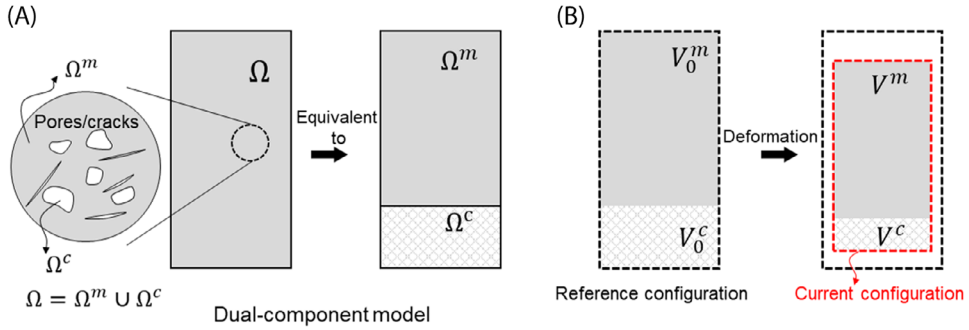

FIGURE 2 Schematic of the proposed model. (A) An equivalent treatment between the original problem and the dual-component model. (B) Volumes in the reference and current configurations.

In the dual-component model, the overall rock domain Ω is comprised of the rock matrix part Ω^m and the pores/cracks part Ω^c, as displayed in Figure 2. Then, the rock specimen is denoted as $\Omega = \Omega^m \cup \Omega^c$. The widely used superposition principle suggests that the overall strain is the sum of the strains from individual components.[34–36]

In particular, we distinguish between the measurement of rock deformation in the reference and current configurations. In the reference configuration, the overall volume is expressed as:

$$V_0 = V_0^m + V_0^c \tag{1}$$

where V_0 is the initial rock volume in an unstressed state. The subscripts m and c denote the matrix and pores/cracks parts, respectively.

In the current configuration, the volume is computed by:

$$V = V^m + V^c,\ dV = dV^m + dV^c \tag{2}$$

where V is the current rock volume, dV is the incremental form.

The fraction of matrix and the fraction of pores/cracks at the initial state are defined as:

$$f_0^m = \frac{V_0^m}{V_0},\ f_0^c = \frac{V_0^c}{V_0} \tag{3}$$

which implies that $f_0^m + f_0^c = 1$. Note that f_0^c represents the volume fraction of the deformed pore space. f_0^c and the initial porosity ϕ_0 are two independent parameters in the model.

2.2 | Rock strain defined in the current configuration

As discussed in Section 1.2, the finite strain theory is well-suited for accurately capturing large deformation in the rock compaction process. The Cauchy stress tensor $\boldsymbol{\sigma}$ and the rate of deformation tensor $\mathbf{D}$ are chosen as the measurements for stress and strain, because they are conjugate in work.[30,31] $\boldsymbol{\sigma}$ is actually the "real stress" in literature,[28,29] while $\mathbf{D}$ represents a generalized form of the "real strain" $\mathbf{e}$.

The finite strain is measured by $\mathbf{D}$, expressed by[30,31]:

$$\mathbf{D} = \frac{1}{2}\left(\mathbf{L} + \mathbf{L}^{\mathrm{T}}\right),\ \text{where } \mathbf{L} = \dot{\mathbf{F}} \cdot \mathbf{F}^{-1} \tag{4}$$

where the velocity gradient tensor $\mathbf{L}$ is determined by the deformation gradient tensor $\mathbf{F}$.

The description of rock deformation varies between the reference and current configurations (Equations 1 and 2). As depicted in Figure 1, We define the Eulerian coordinates $\mathbf{x} = (x_1, x_2, x_3)$ in the reference configuration, and the Lagrangian coordinates $\mathbf{X} = (X_1, X_2, X_3)$ in the current configuration. The deformation gradient tensor $\mathbf{F}$ can be written using the indicial notation[30,31]:

$$F_{ij} = \frac{\partial x_i}{\partial X_j},\ (i, j = 1, 2, 3) \tag{5}$$

The explicit forms of **D**, **L**, and **F** are determined by the patterns of rock deformation, which is relevant to the constitutive relation under specific loading conditions.

2.3 | Constitutive relation in confining pressure state

The motion of a material point within a rock specimen Ω is described by the equations of motion as given in the continuum mechanics:

$$\mathbf{x} = \Phi(\mathbf{X}, t) \tag{6}$$

where the function Φ defines the spatial coordinates **x** of the material point **X** at time t.

For confining pressure state (the hydrostatic pressure), we express Equation (6) in the explicit forms:

$$x_1 = \frac{L(t)}{L^0} X_1,\ x_2 = \frac{L(t)}{L^0} X_2,\ x_3 = \frac{L(t)}{L^0} X_3 \tag{7}$$

where L^0 is the characteristic length in the reference configuration (unstressed state). $L(t)$ is the characteristic length in the current configuration, and it varies with time t. The ratio, denoted as $L(t)/L^0$, represents the stretch. Note that L^0 and $L(t)$ are defined as the maximum lengths of the specimen edges in the reference and current configurations, respectively.

The deformation gradient (Equation 5) is explicitly expressed as:

$$\mathbf{F} = \begin{bmatrix} L(t)/L^0 & 0 & 0 \\ 0 & L(t)/L^0 & 0 \\ 0 & 0 & L(t)/L^0 \end{bmatrix} \tag{8}$$

Therefore, **D** (Equation 4) is written as:

$$\mathbf{D} = \begin{bmatrix} \frac{1}{L(t)}\frac{\partial L(t)}{\partial t} & 0 & 0 \\ 0 & \frac{1}{L(t)}\frac{\partial L(t)}{\partial t} & 0 \\ 0 & 0 & \frac{1}{L(t)}\frac{\partial L(t)}{\partial t} \end{bmatrix} \tag{9}$$

which indicates $\mathbf{L} = \mathbf{L}^{\mathrm{T}}$ and $\mathbf{D} = \mathbf{L}$. Actually, the rate of deformation **D** is exactly equal to the strain rate[30,31]:

$$\mathbf{D} = \frac{\mathrm{d}\mathbf{e}}{\mathrm{d}t} \tag{10}$$

Considering our emphasis on the quasi-static condition, integrating Equation (10) in conjunction with Equation (9), the real strain can be obtained:

$$\mathbf{e} = \begin{bmatrix} \ln(L/L^0) & 0 & 0 \\ 0 & \ln(L/L^0) & 0 \\ 0 & 0 & \ln(L/L^0) \end{bmatrix} \tag{11}$$

The volumetric strain e_v in a confining pressure state is calculated by $e_v = \sum_i e_{ii}, (i = 1, 2, 3)$ and written as:

$$e_v = \ln\left(\frac{[L(t)]^3}{[L^0]^3}\right) = \ln\left(\frac{V}{V_0}\right) \tag{12}$$

where V_0 and V are the volume of rock in the reference and current configurations, respectively. V_0 is a constant value, while V is a stress-dependent variable.

The effective confining stress σ equals to the difference between the confining pressure σ_c and the pore pressure p,[11] that is $\sigma = \sigma_c - n_b p$, where Biot's coefficient n_b is conventionally selected as 1 in this context.[10,11,28]

As suggested by existing literature,[23,28,29] the constitutive relation in a confining pressure state is given by the following formula:

$$\sigma = -Ke_v = -K \ln\left(\frac{V}{V_0}\right) \text{ on } \Omega \tag{13}$$

where the negative symbol indicates volume compression as a positive value, K is the bulk modulus of rock. Equation (13) captures how the current volume of rock V varies with the effective confining pressure σ. Actually, from another perspective, it can be derived through integrating the incremental form $\mathrm{d}\sigma = -K\mathrm{d}e_v$, where the incremental volumetric strain is defined as $\mathrm{d}e_v = \mathrm{d}V/V$.

Applying Equation (13) to both the rock matrix part Ω^m and the pores/cracks part Ω^c, we have:

$$\begin{aligned} \sigma &= -K^m \ln\left(\frac{V^m}{V_0^m}\right) \text{ on } \Omega^m \\ \sigma &= -K^c \ln\left(\frac{V^c}{V_0^c}\right) \text{ on } \Omega^c \end{aligned} \tag{14}$$

where K^m and K^c are the bulk moduli of the rock matrix and the pores/cracks parts, respectively.

The overall volume V of a rock and its incremental form dV in the current configuration (Equation 2) is given by:

$$\begin{aligned} V &= V_0^m e^{-\sigma/K^m} + V_0^c e^{-\sigma/K^c} \\ dV &= -\left[\frac{V_0^m}{K^m} e^{-\sigma/K^m} + \frac{V_0^c}{K^c} e^{-\sigma/K^c}\right] d\sigma \end{aligned} \tag{15}$$

Consequently, a rigors foundation of the FS-DC model is established. Based on this formulation, we can capture the stress-dependent properties during rock deformation, as elaborated in Section 3.

3 | STRESS-DEPENDENT PROPERTIES IN TERMS OF FINITE STRAIN

The stress-dependent properties can be described based on the FS-DC model. These properties are calculated in the current configuration. The finite strain theory performs well in capturing nonlinear behavior compared to the conventional small deformation theory. With appropriate simplifications, the proposed model can be reduced to the existing models.

3.1 | Rock porosity

Variation in rock porosity ϕ reflects changes in the volume of pores and cracks. In a compression process, porosity is a stress-dependent quantity that consistently decreases as the confining pressure increases. An accurate definition of rock porosity should be associated with the current configuration rather than the reference configuration. An accurate definition of rock porosity is $\phi = V^c/V$.[23] We formulate the incremental form as:

$$\frac{\mathrm{d}\phi(\sigma)}{\mathrm{d}\sigma} = \frac{1}{V(\sigma)} \frac{\mathrm{d}V^c(\sigma)}{\mathrm{d}\sigma} - \frac{V^c(\sigma)}{(V(\sigma))^2} \frac{dV(\sigma)}{d\sigma} \tag{16}$$

which implies that ϕ, V and V^c are functions of σ. Remarkably, to the best of our knowledge, Equation (16) presents a perspective not found in existing literature. Here, ϕ is defined in relation to the stress-dependent volume V in the current configuration.

Notably, some authors[28,29] computed porosity using $\mathrm{d}\phi = \mathrm{d}V^c/V_0$, which differs from our formulation ($\mathrm{d}\phi = \mathrm{d}V^c(\sigma)/V(\sigma)$). In addition, they neglected the second term on the left-hand side of Equation (16), which accounts for the change in V.

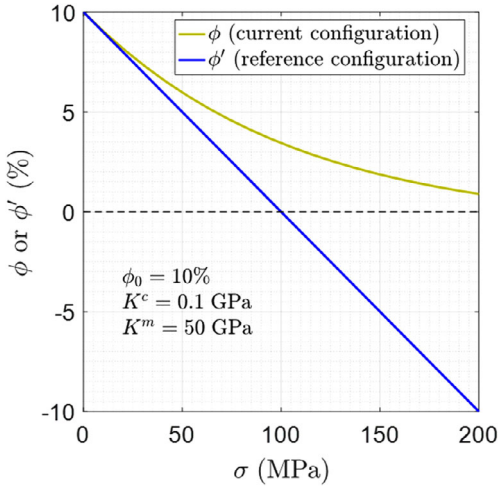

FIGURE 3 Comparison of different measurements of porosity (Equations 17 and 19) with an increasing effective confining pressure σ.

Substituting Equation (15) into (16), and integrating it with the condition $\phi = \phi_0$ at $\sigma = 0$, the porosity in the current configuration is formulated as:

$$\phi = \phi_0 - f_0^c + \frac{f_0^c e^{-\sigma/K^c}}{f_0^c e^{-\sigma/K^c} + f_0^m e^{-\sigma/K^m}} \tag{17}$$

where ϕ_0 is the initial porosity in unstressed state. If deformation of the rock matrix can be neglected in comparison to that of micro-cracks ($K^m \gg K^c$ and $K^m/(K^m - K^c) \approx 1$), Equation (17) can be simplified to the model presented in existing literature.[28,29,38–40]

Moreover, in the reference configuration, the porosity, denoted as ϕ', can be directly formulated as:

$$\mathrm{d}\phi' = \frac{\mathrm{d}V^c(\sigma)}{V_0}, \text{ where } V^c(\sigma) = V_0^c\left(1 - \frac{\sigma}{K^c}\right) \tag{18}$$

After integration, ϕ' is expanded as:

$$\phi' = \phi_0 - \frac{f_0^c}{K^c}\sigma \tag{19}$$

which indicates that in the reference configuration, porosity is purely dependent on σ and pores/cracks properties (f_0^c and K^c).

Figure 3 depicts the variation of porosity with varying σ to illustrate the differences between Equations (17) and (19). This demonstrates that ϕ' will exhibit unphysical behavior (negative values) at high levels of σ. In contrast, ϕ is capable of capturing the behavior in a more physical way, where it decreases nonlinearly with increasing confining pressure. A comprehensive analysis of the experimental results using the proposed model will be presented in Section 6.

Equation (17) establishes a connection between the variation of ϕ and σ in the current configuration. All parameters possess specific physical interpretations, and can be determined through experiments or via curve fitting. The method for determining model parameters will be elaborated in Section 4.

3.2 | Volumetric strain

The utilization of real strain e_v and engineering strain E_v may produce considerable differences in predicating volume variation of rocks. To illustrate this point, a comparative analysis is given as follows.

The real strain e_v defined in the current configuration is given by Equation (12), while the engineering strain E_v defined in the reference configuration is expressed as:

$$E_v = -\left(\frac{V}{V_0} - 1\right) \tag{20}$$

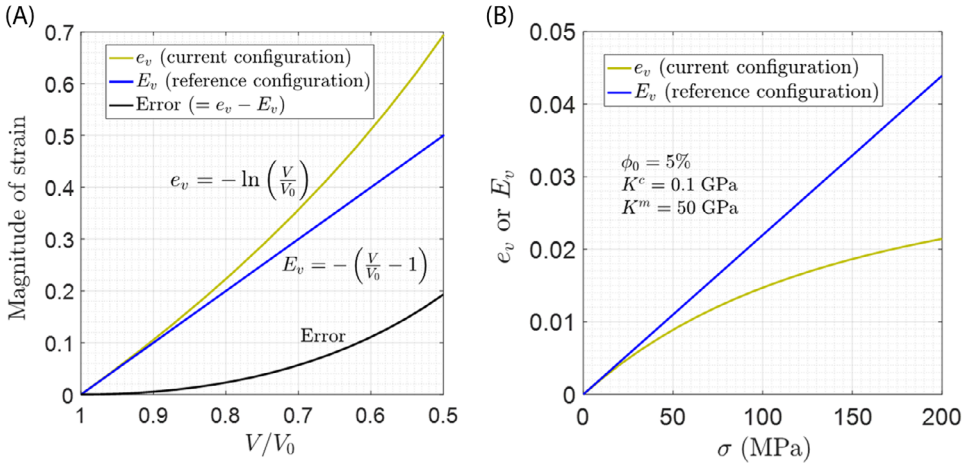

FIGURE 4 Comparison of different measurements of volumetric strain (Equations 12, 20, and 22). V_0 and V are the initial and current volumes of rock, respectively.

As illustrated in Figure 4A, the ratio V/V_0 represents the fraction of current volume V accounted for by the initial volume V_0. Remarkably, the relation between V/V_0 and e_v is nonlinear, and as V/V_0 increases, e_v experiences a rapid rise, while the curve $V/V_0 - E_v$ remains linear even at high values of V/V_0. It shows that E_v tends to underestimate the true strain in comparison to e_v. This effect becomes more pronounced when there is a significant volumetric change during rock compression.

Equations (12) and (20) cannot account for the stress-dependent feature of strain. To achieve this, the stress-dependent volumetric strains e_v and E_v can be expressed through an analogy to Equation (16):

$$\frac{\mathrm{d}e_v(\sigma)}{\mathrm{d}\sigma} = -\frac{1}{V(\sigma)}\frac{\mathrm{d}V(\sigma)}{\mathrm{d}\sigma}, \quad \frac{\mathrm{d}E_v(\sigma)}{\mathrm{d}\sigma} = -\frac{1}{V_0}\frac{\mathrm{d}V(\sigma)}{\mathrm{d}\sigma} \tag{21}$$

Then, using Equation (15), the two different measurements of volumetric strain in Equation (21) are reformulated as:

$$\begin{aligned} e_v &= e_0 + \ln\left(f_0^m e^{-\sigma/K^m} + f_0^c e^{-\sigma/K^c}\right) \\ E_v &= E_0 + \left(\frac{f_0^m}{K^m} + \frac{f_0^c}{K^c}\right)\sigma \end{aligned} \tag{22}$$

where e_0 and E_0 are the initial strains in the current and reference configurations, respectively. Figure 4B demonstrates that E_v varies linearly with σ, which is incorrect at low confining pressure. The results presented by Watanabe and Higuchi[13] suggest that the volumetric strain of biotite granite is nonlinear when $\sigma < 50$ MPa. The nonlinear behavior arises from the closure of micro-cracks. Equation $(22)_1$ can capture such feature more accurately than Equation $(22)_2$.

3.3 | Rock compressibility and specific storage

Rock bulk compressibility, denoted as C_b, quantifies ability of rock to deform with a confining pressure σ. It characterizes changes in rock volume as σ increases. We follow the definition of compressibility proposed by Zimmerman.[23] Under conditions of constant pore pressure, it is expressed as:

$$C_b = -\frac{1}{V_0}\frac{\partial V}{\partial \sigma} \tag{23}$$

where the term $\partial V/\partial\sigma$ can be obtained from Equation $(15)_2$. The explicit form of C_b can be directly derived:

$$C_b = \frac{f_0^m}{K^m}e^{-\sigma/K^m} + \frac{f_0^c}{K^c}e^{-\sigma/K^c} \tag{24}$$

Moreover, pore compressibility, denoted as C_p, can be defined in a manner analogous to C_b:

$$C_p = -\frac{1}{V_0^c}\frac{\partial V^c}{\partial \sigma} \tag{25}$$

Following the same procedure used to derive Equation (24), we obtain the explicit form of pore compressibility:

$$C_p = \frac{1}{K^c} e^{-\sigma/K^c} \tag{26}$$

Equations (24) and (26) provide C_b and C_p in the current reference based on the FS-DC model. The formulas are consistent with the existing results.[28,29] Here, we select three facts to illustrate this point: (1) If the rock matrix is assumed to be stiffer than the micro-cracks ($K^m \gg K^c$), the approximation $e^{-\sigma/K^m} \approx 1$ is valid. Then, Equation (24) can be degenerated into the result given by Liu et al.[28] (Equation 12 in their paper). (2) Zimmerman[23] and Jaeger et al.[41] also used similar exponential functions to analyze their experimental results. (3) Applying Reuss averaging method[41,42] to the rock matrix and micro-cracks parts, the same expression as in Equation (24) can be obtained.

Specific storage, denoted as S_s, captures the ability of a rock formation to store fluid within its pores or cracks. The definition is expressed as[7,43]:

$$S_s = \frac{C_p}{1-\phi} + \phi(C_s + C_f) \tag{27}$$

where C_s and C_f is the compressibilities of solid grains and pore fluid, respectively. C_s can be neglected as it is very small ($\sim 10^{-5}$ MPa^{-1}) compared to C_p and C_f. For conciseness, Shi and Wang[44] reformulated Equation (27) as follows:

$$S_s = C_b + \phi C_f \tag{28}$$

where ϕ and C_b are stress-dependent quantities and determined by (17) and Equations (24), respectively.

3.4 | Effective permeability of porous rocks

Rock permeability quantifies the ability of fluid to flow through rocks, resulting from the contributions from both the rock matrix and the pores/cracks parts. The effective permeability k_{eff} is an important parameter that reflects the overall hydraulic property of rocks.

There are various forms of the connection between k_{eff} and σ. The majority of these relations are empirical relations, such as exponential and power laws.[9,10,22] However, parameters in existing models lack of physical significance and cannot be properly correlated with σ. We utilize the Kozeny–Carman relation,[45,46] where the porosity ϕ acts as a bridge connecting σ and k_{eff}:

$$\frac{k_{eff}}{k_r} = \left(\frac{\phi(\sigma)}{\phi_r}\right)^m \tag{29}$$

where $\phi(\sigma)$ is the stress-dependent porosity, determined by Equation (17). k_r and ϕ_r are reference values of permeability and porosity. k_{eff} can be further written in a more compact form:

$$k_{eff} = \alpha \phi^m \tag{30}$$

where m and α are coefficients determined through curve fitting, and $\alpha = k_r/(\phi_r)^m$. ϕ is calculated in the current configuration based on the FS-DC model, denoted as $\phi = \phi(\sigma)$. Then, the complete expression of k_{eff} is written as:

$$k_{eff} = \alpha \left(\phi_0 - f_0^c + \frac{f_0^c e^{-\sigma/K^c}}{f_0^c e^{-\sigma/K^c} + f_0^m e^{-\sigma/K^m}} \right)^m \tag{31}$$

4 | MODEL PARAMETERS

The proposed FS-DC model provides a formulation capable of interpreting variations in stress-dependent properties of rocks. Table 1 presents the parameters involved in the model for calculating various properties. Several parameters can be

TABLE 1 Parameters in the finite strain-based dual-component model.

Stress-dependent properties	All parameters	Experimental data	Equations in FS-DC model
Porosity ϕ	ϕ_0, K^m, K^c, f_0^c	ϕ_0	Equation (17)
Volumetric strain e_v	e_0, K^m, K^c, f_0^c	-	Equation $(22)_2$
Bulk compressibility C_b	K^m, K^c, f_0^c	-	Equation (24)
Pore compressibility C_p	K^c	-	Equation (26)
Specific storage S_s	$\phi_0, K^m, K^c, f_0^c, C_f$	ϕ_0, C_f	Equation (28)
Effective permeability k_{eff}	$\phi_0, K^m, K^c, f_0^c, m, \alpha$	ϕ_0	Equation (30)

Remarks. (1) "Experimental data" are the parameters that can be obtained from experiments. (2) We choose either f_0^m or f_0^c as a parameter, as they are not independent ($f_0^m + f_0^c = 1$). (3) C_f can be set equal to the compressibility of water (4.5×10^{-4} MPa^{-1}) or nitrogen gas (7.1 MPa^{-1}) when calculating S_s. (4) e_0 is typically assumed to be 0 under unstressed condition.

TABLE 2 Data source from different experiments.

	Rock type	Maximum σ	Permeability measurement	Sampling spot
Dong et al.[10]	Fine-grained shale, Silty-sandstone	120 MPa	Steady flow, nitrogen gas	Chelungpu fault drill hole
Watanabe and Higuchi[13]	Fine-grained granite	180 MPa	-	Aji, Kagawa
Ghabezloo et al.[11]	Limestone	20 MPa	Steady flow, water	Near Nîmes
Zimmerman[23]	Sandstone	30 MPa	-	-
David et al.[9]	Sandstone	550 MPa	Steady flow, transient pulse	Île-de-France and Vosges

Remarks. (1) "Maximum σ" refers to the highest level of the confining pressure employed in experiment. (2) The symbol "-" indicates that there is no information available in literature regarding this item.

directly measured in experiments, such as the initial porosity ϕ_0. However, in many scenarios, parameters such as m, α and f_0^c need to be determined through curve fitting based on experimental data.

Physical interpretations of model parameters in the FS-DC model are discussed as follows:

- ϕ_0 is the initial porosity under unstressed condition. It is a constant.
- K^m and K^c are the bulk moduli of the rock matrix and the pores/cracks parts, respectively. They represents the stiffness of a materials and their ability to deform.
- f_0^c denotes the fraction of pores/cracks V_0^c that have the potential to deform, relative to the initial overall volume V_0. f_0^c is a constant since it is defined in the initial unstressed state.
- m is the porosity sensitivity exponent, which has also been discussed in Refs. [9, 29]. It signifies the rate of change in porosity with respect to confining pressure.
- α is a coefficient that reflects the combined effect of the reference values of permeability k_r and porosity ϕ_r, expressed as $\alpha = k_r/(\phi_r)^m$.
- Among these parameters, except for the initial porosity ϕ_0 and the compressibility of pore fluid C_f can be obtained from experiments, others should be determined by curve fitting based on the analysis of experimental data.

The methods for determining model parameters is a special subject in data analysis. Optimization methods are essential when the model incorporates numerous undetermined parameters lacking explicit physical interpretations.[47–49] The proposed FS-DC model has only a few parameters, and these parameters possess specific physical explanations. We can also provide rough estimates for the range of some parameters derived from practical experiences. In this study, the well-established nonlinear least squares method is utilized for curve fitting,[50] where the Levenberg-Marquardt method is adopted to improve accuracy.

5 | EXPERIMENT DESCRIPTION AND DATA SOURCE

In this study, our emphasis is not on delving into the details in experiments. Instead, we use these published experimental results to explore the performance of the FS-DC model and its implications in rock properties. Descriptions of data source and different experiments are given in Table 2.

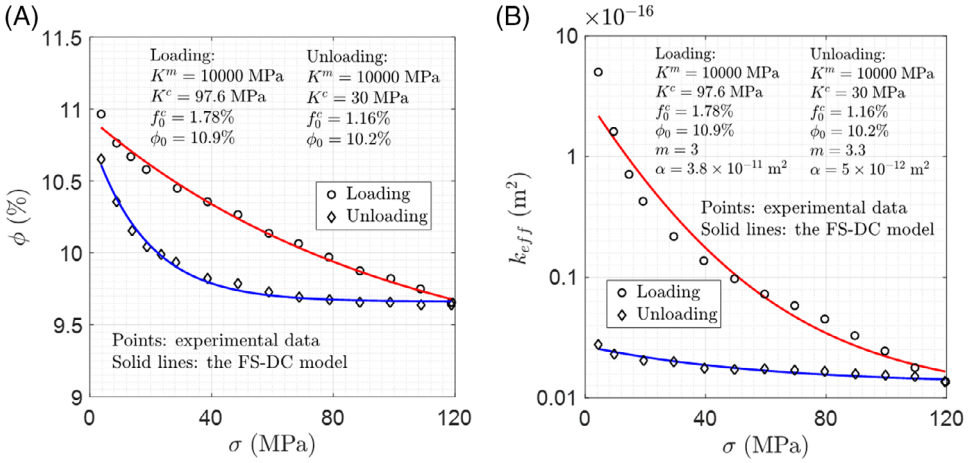

FIGURE 5 Comparison of variation in porosity and permeability obtained from experiments (silty-shale)[10] and the FS-DC model. FS-DC, finite strain-based dual-component.

Many authors have conducted rock compaction experiments on various types of rocks, to analyze changes in stress-dependent permeability, porosity, and compressibility as the effective confining pressure increases.[9–11,23,24] These experiments focus on different aspects of rock properties, and have differences in measuring changes in permeability using the steady flow method[10,11] or the transient pulse method.[7,9,24] The pore fluid used for measuring permeability can be either nitrogen gas or water. The experiments are conducted under diverse confining pressure varying within a limited range. Rock permeability and porosity are measured at different stages corresponding to the increasing confining pressure.

As shown in Table 2, the majority of the experiments were conducted on sedimentary rocks (shale and sandstone), with a smaller portion focusing on metamorphic rocks (limestone). Notably, the confining pressure in experiment conducted by David et al.[9] was at a very high level (~550 MPa), as they were intended to mimic the extreme ground pressure conditions in the environment of Earth's crust. Actually, the variations of the stress-dependent properties are complicated, as the inherent properties of rocks at great depths, in rheological state, are distinct from those in the shallow subsurface. In addition, micro-cracks play a crucial role in this context. Based on the existing experimental results, we will discuss the validation of the FS-DC model across a wide range of confining pressure. The distinctions of rock properties under conditions of $\sigma < 200$ MPa and > 300 MPa are studied, as detailed in Section 6.

6 | RESULTS AND DISCUSSION

In this section, the FS-DC model is utilized to analyze the variations in stress-dependent properties of rocks based on the experimental results for different rock types. The effects of pores/cracks and rock bulk properties are deeply explored, with a particular emphasis on examining the applicability of the FS-DC model under extremely high pressure conditions.

6.1 | Porosity and permeability in loading and unloading conditions

Experimental studies have revealed distinct characteristics in the porosity ϕ and permeability k_{eff} of rocks under loading and unloading conditions.[10] These observations can be attributed to the irreversible processes taking place within the rock materials. Alterations in the micro-structure of rock skeleton play a crucial role in this phenomenon. While the proposed FS-DC model is a macroscopic phenomenological model, it can capture such irreversible behavior of variation in ϕ and k_{eff} during loading and unloading processes. We utilize the experimental data reported in Ref. [10], as detailed in Table 2, to examine the performance of the FS-DC model.

Figures 5 and 6 depict how ϕ and k_{eff} change as the effective confining pressure σ increases for the silty-shale and the fine-grained sandstone. It demonstrates that the FS-DC model well reproduces the experimental results. The model parameters possess physical meanings and their magnitudes fall in a reasonable range. The bulk modulus K^m is considerably higher than the pores/cracks modulus K^c, with K^m remaining constant throughout both the loading and unloading

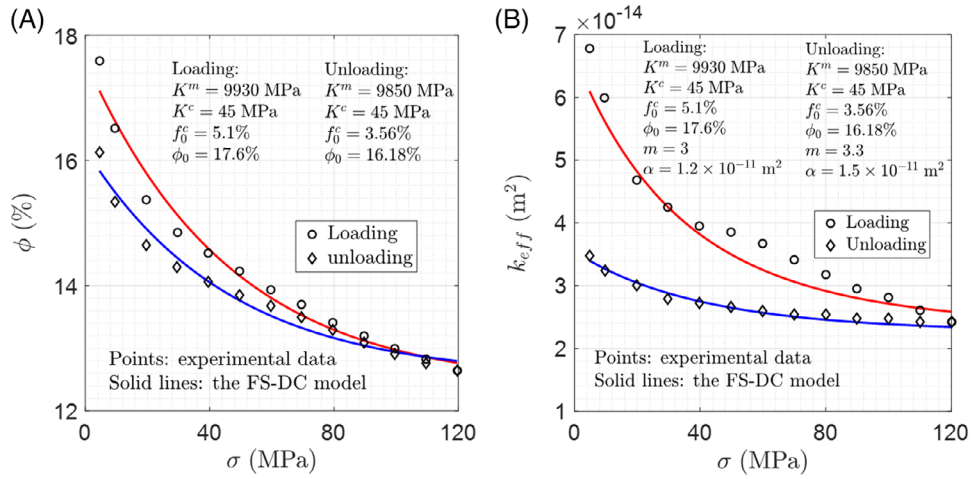

FIGURE 6 Comparison of variation in porosity and permeability obtained from experiments (fine-grained sandstone)[10] and the FS-DC model. (FS-DC, finite strain-based dual-component)

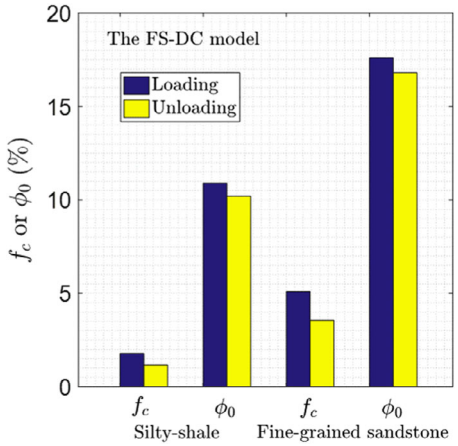

FIGURE 7 Decrease of model parameters (f_0^c and ϕ_0) under loading and unloading conditions, corresponding to Figures 5 and 6.

processes. In contrast, K^c experiences substantial decreases in the case of silty-shale, while it remains nearly unchanged in the fine-grained sandstone.

Especially, the change in permeability due to the reduction in crack aperture (indicated by reduced porosity) is expected to conform to the well-known cubic law,[51] which suggests that the porosity sensitivity exponent m should be approximately 3. As shown in Figures 5 and 6, it is observed that m is indeed close to 3, consistent with the exponent of the cubic law. This point has been also discussed in Refs. [9, 29]. They pointed out that some authors employed the empirical laws for curve fitting with a very large m (even m =70.17), which violates the cubic law.

Model parameters differ between the loading and unloading processes due to the decrease of ϕ and k_{eff}. Variations of the pores/cracks fraction f_0^c and the initial porosity ϕ_0 are displayed in Figure 7. Physically, it can be explained by the fact that closure and breakage of micro-cracks result in a reduction in pore spaces, which is an irreversible phenomenon.

As illustrated in Figure 8, Ghabezloo et al.[11] investigated the relation between k_{eff} and the confining pressure σ_c for limestone. Note that σ_c equals to $\sigma + p$, as given in Section 2.3. With an increasing pore pressure p, the effective permeability k_{eff} increases as well. Additionally, permeability of limestone ($\sim 1 \times 10^{-17}$ m^2) is lower than that of silty-shale ($\sim 1 \times 10^{-16}$ m^2) and fine-grained sandstone ($\sim 1 \times 10^{-14}$ m^2).

Moreover, to deeply investigate the effect of pore pressure on rock properties, various effective stress coefficients can be defined for permeability, porosity, pore and bulk volume strains, as suggested in Refs. [52, 53]. The determination of the effective stress coefficient for permeability, denoted as n_k, which can even exceed 1, has long been a subject of significant

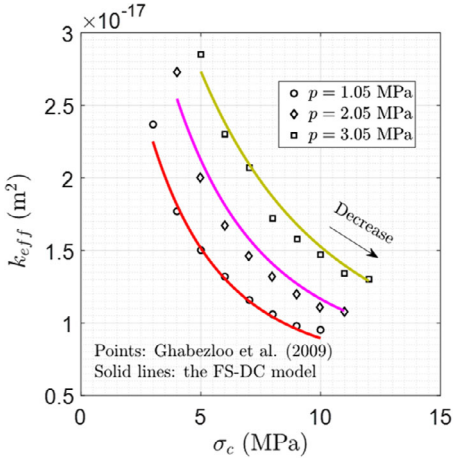

FIGURE 8 Correlation between permeability (limestone) and increasing confining pressure. The experimental data is extracted from Ref. [11].

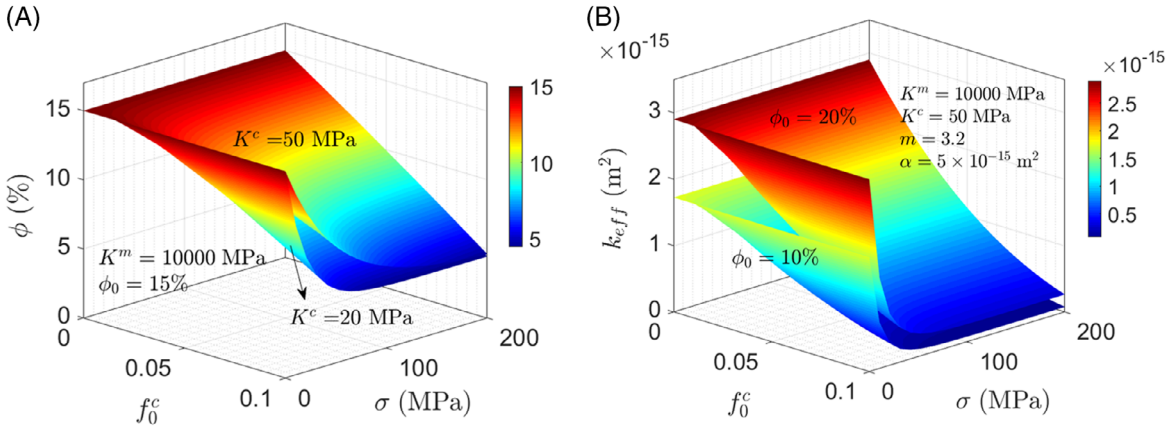

FIGURE 9 Variation of porosity and permeability with various pores/cracks properties (f_0^c and K^c) and increasing effective confining pressure.

interest. As an illustration, we follow the method proposed in Ref. [52] to calculate n_k for Figure 8. n_k is calculated by:

$$n_k = \left.\frac{\partial \sigma_c}{\partial p}\right|_{k_{eff}=\text{const.}} \tag{32}$$

In Figure 8, the increment of pore pressure Δp is 1 MPa. Fixing the permeability k_{eff} and shifting a curve, a satisfactory alignment among the curves is achieved when $\Delta\sigma_c = 2.45$ MPa. The coefficient is calculated as $n_k = \Delta\sigma/\Delta p = 2.45$.

6.2 | Effect of pores/cracks properties

The pore spaces within rocks comprise both micro-pores and cracks. In the FS-DC model, the volume fraction f_0^c and the modulus K^c are associated with characteristics of these pores and cracks. Figure 9A shows the relation between f_0^c and ϕ as σ increases. When $\sigma = 0$, ϕ remains constant, signifying the absence of deformation within the pore spaces. This observation is consistent with the actual behaviors exhibited by porous rocks. The increase in K^c does not obviously affect ϕ at very low and high levels of σ. As an illustration, the value of ϕ remains nearly constant regardless of whether K^c is 20 or 40 MPa when σ is maintained at 200 MPa. This variation also depends on the initial porosity ϕ_0 and bulk modulus K^m, and the influence of K^m can be neglected if its value is significantly larger (for instance 10,000 MPa) compared to K^c.

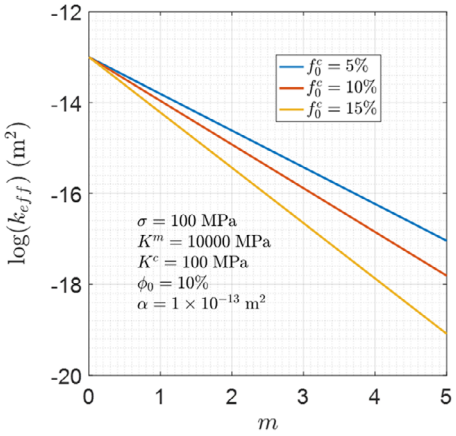

FIGURE 10 Effect of the porosity sensitivity exponent m and the pores/cracks fraction f_0^c on effective permeability k_{eff}.

Figure 9B demonstrates that the impact of ϕ_0 on k_{eff} is correlated with f_0^c. When f_0^c is relatively small ($f_0^c < 0.05$), an increase in ϕ_0 significantly improves k_{eff}. However, if f_0^c is relatively high ($f_0^c > 0.1$), the variation in k_{eff} becomes less pronounced even with alterations in ϕ_0 (ranging from 10% to 20%). k_{eff} approaches a stable value as σ increases. An underlying fact is that there is no extra space available for the closure of micro-cracks, and the volume of pores and cracks tends to remain constant.

The exponent m in Equation (30) represents the sensitivity of permeability to rock porosity. Previous studies have pointed out that even a small change in m can significantly impact permeability.[9,11] To explain this phenomenon, Figure 10 illustrates the relation between m and permeability. The y-axis is scaled by logarithm, while the x-axis ranges from 0 to 6. It is evident that the variation of $\log(k_{eff})$ exhibits a nearly linear decrease as m increases. Notably, the permeability of a rock with a relatively large f_0^c (=15%) is lower than that of a rock with a smaller f_0^c (=5%). Comparing the curve slopes of $f_0^c = 5\%$ and 15%, it implies that porous rock is more sensitive to variations in m compared to more denser rock. The reason is that the pore spaces undergo compression under confining pressure, leading to a more pronounced reduction in k_{eff} as f_0^c increases.

6.3 | Compressibilities, volumetric strain and specific storage

Compressibilities C_b and C_p quantify the capacity for deformation of pores and the bulk rock under confining pressure. Zimmerman[23] conducted a comprehensive investigation into the compressibility of sandstone using a combination of experimental and theoretical approach. Based on the findings presented in Refs. [12, 23] Figure 11A provides the variation in C_b with an increase in effective confining pressure σ. In this scenario, C_b tends to a constant value after σ >20 MPa. The pressure level is relatively low because the modulus of pores is very small ($K^c = 4.9$ MPa). Therefore, the micro-pores and cracks close rapidly even under a low pressure condition.

Figure 11B illustrates the relation between C_p and the confining pressure σ_c. Different values of pore pressure p have a significant impact on the compressibility properties of the pores. It is found that higher values of p can improve compressibility. This observation aligns with real-world rocks, wherein an increase in pore pressure enhances the resistance of rock to compressive deformation. Regardless of the value of p, C_p approaches a constant value beyond a certain σ_c. In Figure 11B, the value of σ_c is 35 MPa, which is sufficiently larger than p (=15.45 MPa). Actually, it can be inferred that the variations in both C_b and C_p will tend to stabilize when the confining pressure is sufficiently high.

To further analyze the effect of pores/cracks properties on rock bulk compressibility, Figure 12 presents a 3D surface depicting variations in f_0^c and K^c. When K^c is very small (<10 MPa), changes in f_0^c ($0 \sim 0.1$) do not significantly impact C_b, regardless of the value of σ. It is attributed that a small K^c represents a softer material, which in turn makes the pore spaces more susceptible to compression. On the contrary, when K^c is a higher magnitude (>50 MPa), a slight increase in f_0^c could enhance the compressibility. This influence becomes negligible at sufficiently high values of σ.

In an experimental study by Watanabe and Higuchi,[13] the relation between an increasing σ and the volumetric strain e_v was measured, as depicted in Figure 13A. The proposed FS-DC model accurately reproduces this experimental result. At low levels of σ, the relation exhibits nonlinearity, transitioning to linearity for σ >50 MPa. Figure 13B shows the influences

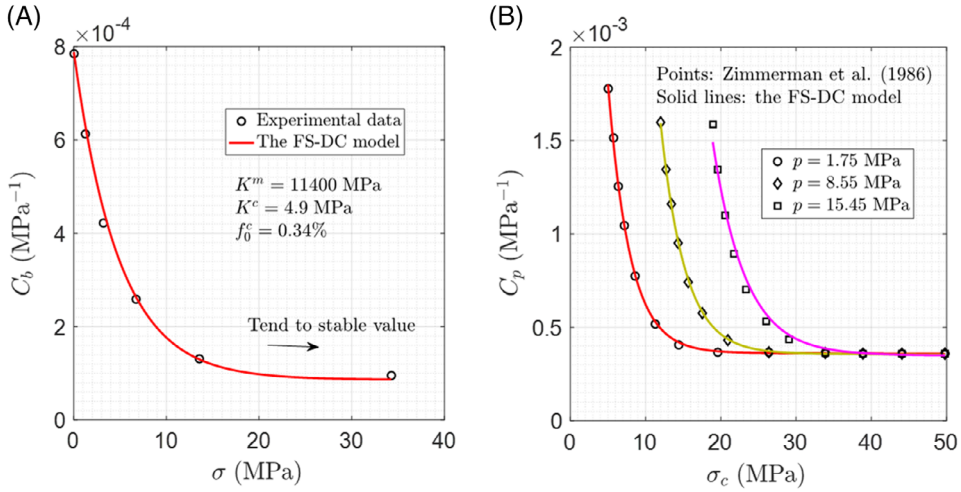

FIGURE 11 Comparison of bulk and pore compressibilities (C_b and C_p) between experimental data (sandstone)[12,23] and the FS-DC model. FS-DC, finite strain-based dual-component.

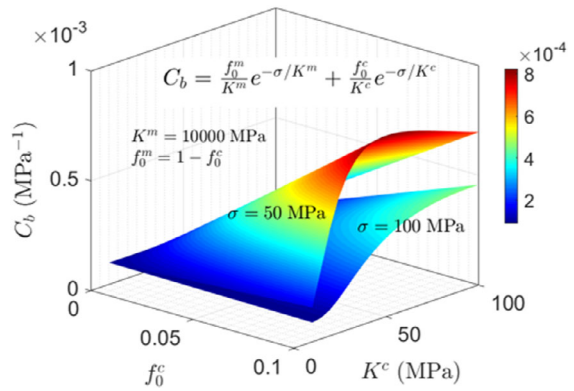

FIGURE 12 Effect of pores/cracks properties on bulk compressibility.

of f_0^c and K^c on volumetric strain. These properties exhibit contrasting effects. A low value of K^c corresponds to a softer material that is more prone to deformation. Conversely, a reduced f_0^c leads to a stiffer material, as the volume of pores and cracks becomes too small.

The variation in specific storage S_s is closely related to compressibility, which is formulated as $S_s = C_b + \phi C_f$ (Equation 28). It represents the combined effect of porosity and compressibilities of rock bulk and pore fluid. By comparing Figures 11A and 14A, it becomes apparent that the S_s-σ and C_b-σ curves exhibit similarities. Both S_s and C_b will converge to stable constants if σ is sufficiently large. This observation can be explained by a view of micro-structure, where the closure and breakage of pores and cracks play a significant role. The FS-DC model captures these characteristics of the micro-structure in a phenomenological manner through several macro-scale variables (f_0^c, K^c, and ϕ_0). In the experiment conducted in Ref. [10], the pore fluid is nitrogen gas, and C_p is a fixed value (7.1 MPa^{-1}). Figure 14B shows the relations between S_s and K^c with various f_0^c and ϕ_0. Obviously, increase in ϕ_0 enhances S_s, as the volume of pore spaces increases as well. The effect of K^c is more pronounced at low levels of σ (<40 MPa) than at higher levels (>80 MPa).

6.4 | Extremely high confining pressure

Previous studies have shown that rock properties at high confining pressure (σ > 300 MPa) differ from those observed under the relatively low pressure conditions (σ < 200 MPa). Experiments on rock compaction conducted at extremely high pressure levels have received limited attention in comparison to studies conducted at lower pressure levels. Notably, David et al.[9] carried out a comprehensive investigation into the stress-induced variations in permeability and porosity. In

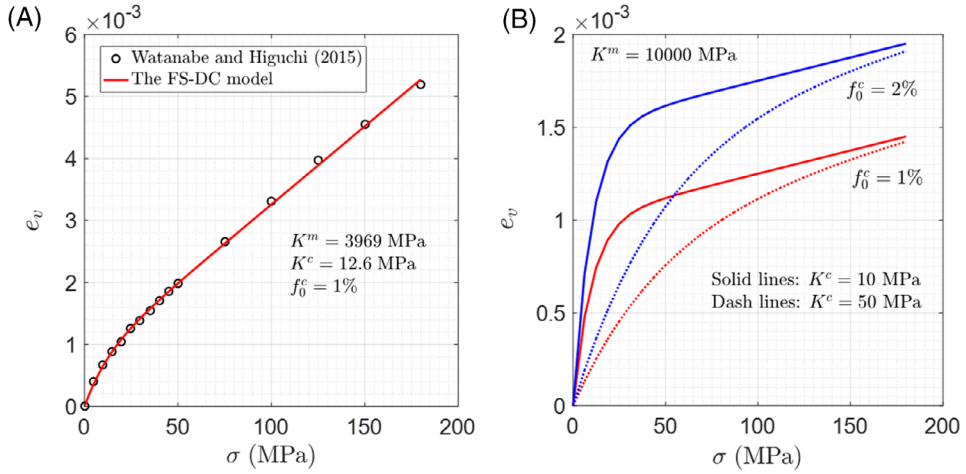

FIGURE 13 Comparison of volumetric strain e_v between experimental data (fine-grained granite)[13] and the FS-DC model. FS-DC, finite strain-based dual-component.

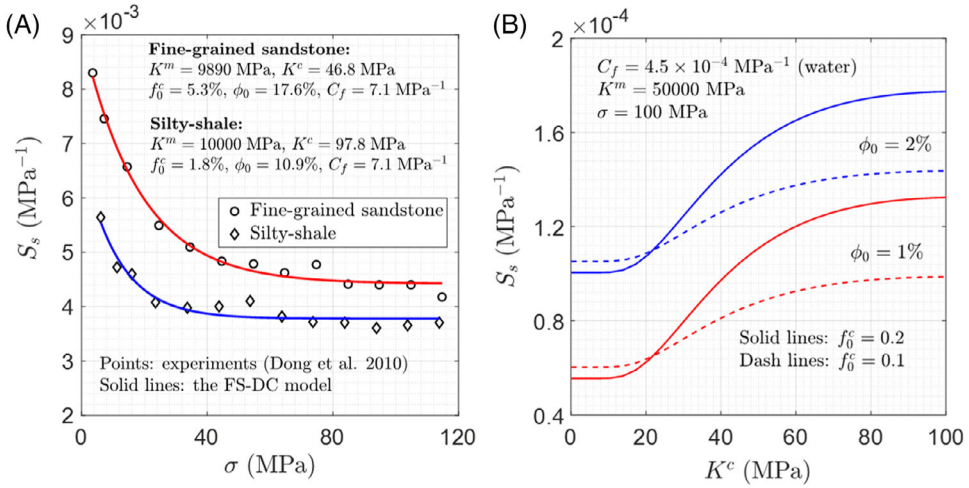

FIGURE 14 Comparison of specific storage S_s between experimental data (sandstone and shale)[10] and the FS-DC model. FS-DC, finite strain-based dual-component.

their experiment, the confining pressure level reaches up to 550 MPa, with the aim of simulating subsurface conditions found in deep underground environments.

Based on the results reported in Ref. [9], Figures 15A and 16A illustrate the variations in permeability and porosity with increasing stress for Berea sandstone, Adamswiller sandstone, and Rothbach sandstone. The FS-DC model can approximately replicate these observations, however the discrepancy becomes significant at the high level of σ. This is because the micro-structure of rocks undergoes fundamental alterations under extremely high pressures, resulting in inelastic deformation. The rock skeleton experiences permanent deformation and breakage.

To improve accuracy, the discrepancy between the experimental data and the results obtained from the FS-DC model can be properly eliminated through piecewise fitting. The curves displayed in 15B and 16B are predicted using the piecewise fitting based on the FS-DC model, where the two piecewise curves are denoted as C2-1 and C2-2. The curves predicted using the FS-DC model without piecewise fitting are denoted as C1, as displayed in Figures 15A and 16A. Parameter values are given in Table 3.

Analogy to David et al.,[9] where their introduced the concept of the critical pressure (the pressure at which k_{eff} abruptly changes), we define the initiation points at which micro-cracking occurs. P_1, P_2, and P_3 shown in Figure 15B are these points for the three different types of sandstone. It can be observed that prior to the initiation points, the variation in k_{eff} follows a similar pattern as seen in the majority of experimental results, for instance, Figures 5B, 6B, and 8.

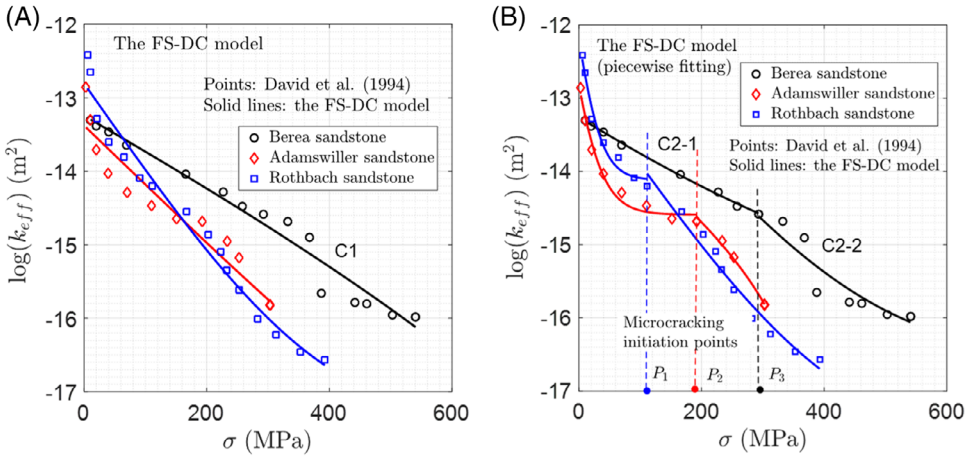

FIGURE 15 (A) Permeability of three types of sandstone under extremely high effective confining pressure (up to 550 MPa). The experimental data is extracted from Ref. [9]. (B) Permeability variation predicted by the FS-DC model (piecewise fitting).

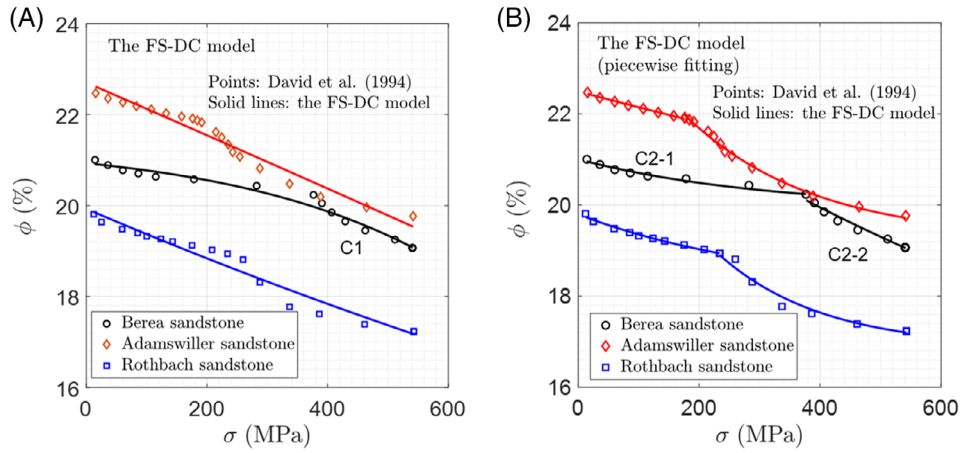

FIGURE 16 (A) Porosity of three types of sandstone under extremely high effective confining pressure (up to 550 MPa). The experimental data is extracted from Ref. [9]. (B) Porosity variation predicted by the FS-DC model (piecewise fitting). FS-DC, finite strain-based dual-component.

Similar to permeability, the variation of porosity exhibits different behaviors at different levels of σ. Figure 16A shows that the relation between ϕ and σ is almost linear, but not a strict linear relation. With the piecewise fitting, the FS-DC model effectively reproduces the experimental results, as illustrated in Figure 16B. This nonlinearity can be attributed to the inelastic deformation of micro-pores and cracks under extremely high σ.

7 | CONCLUSIONS AND OUTLOOK

In this work, we investigated the characteristics of stress-dependent properties during rock deformation processes. A novel FS-DC model was proposed to interpret the correlations among the permeability, porosity, and compressibility of rocks. The main concluding remarks and implications are summarized as follows:

(1) The FS-DC model conceptualizes the original problem as a combination of the rock matrix and micro-pores/cracks parts. The formulation is based on finite strain theory, using the concept of the deformation gradient tensor within the framework of continuum mechanics. The quantities are calculated in the current configuration, as opposed to the reference configuration in conventional methods.

TABLE 3 Values of parameters in the FS-DC model.

	Berea sandstone			Adamswiller sandstone			Rothbach sandstone			Unit
	C1	C2-1	C2-2	C1	C2-1	C2-2	C1	C2-1	C2-2	
K^m	9000	9000	8300	8900	8800	8360	6200	7700	6110	[MPa]
K^c	44	37.8	46	26.1	26.2	36.6	15.5	32.3	10.7	[MPa]
f_0^c	19	15	17	19	10	18	16	12	17	[%]
ϕ_0	21	21	21	22	21	21	20	20	20	[%]
m	4.6	5.3	3.7	5.2	5.3	4.6	5.4	4.9	4.4	[-]
α	1.5	2.5	9.9	5.5	8.5	5.9	9.8	9.6	9.7	[$\times 10^{-10}$ m^2]

Remarks. (1) "C1" refers to the curves predicted by the FS-DC model. "C2-1" and "C2-2" represent the piecewise curves 1 and 2 predicted by the FS-DC model (piecewise fitting). (2) All parameters listed in the table are involved in Figure 15, while only K^m, K^c, f_0^c, and ϕ_0 are involved in Figure 16.

(2) The FS-DC model has a few number of parameters, each with specific physical interpretations. With appropriate simplifications, the FS-DC model can be reduced to existing models. An accurate method for determining model parameters was introduced to enhances the accuracy of the curve fitting results.
(3) The performance of the FS-DC model was examined against existing experimental data, including permeability, porosity, compressibility, volumetric strain and specific storage. The results demonstrate that the model efficiently captures the irreversible changes in permeability and porosity during loading and unloading processes. The model outperforms the conventional deformation theory, particularly in capturing nonlinear behaviors.
(4) Further analysis reveals the effect of pores/cracks parameters on the stress-dependent properties. We examined the applicability of the FS-DC model across a wide range of pressures. The findings reveal notable distinctions in rock properties at high confining pressure ($\sigma > 300$ MPa) compared to relatively low pressure conditions ($\sigma < 200$ MPa). This disparity can be attributed to alterations in the micro-structure of rocks under extremely high pressures, resulting in inelastic behaviors characterized by permanent deformation and breakage in rock skeleton.

Ongoing research are focused on incorporating the temperature effect and providing a quantitative description of micro-cracks. We plan to integrate the FS-DC model into our simulation program[36,54,55] for application in geotechnical engineering and geomechanical processes.

AUTHOR CONTRIBUTIONS

Luyu Wang: Conceptualization; methodology; data curation; validation; formal analysis; writing—original draft. **Yanjun Zhang**: Formal analysis; data curation; writing—review and editing.

ACKNOWLEDGMENTS

The authors are grateful to Professor Robert Zimmerman of Imperial College for his helpful discussions and encouragement. This work was financially supported by National Natural Science Foundation of China (No. 52304039).

CONFLICT OF INTEREST STATEMENT

The authors declare that they have no known competing financial interests or personal relationships that could have appeared to influence the work reported in this paper.

DATA AVAILABILITY STATEMENT

Data will be made available on request.

ORCID

Luyu Wang https://orcid.org/0000-0003-2882-3503

REFERENCES

1. Chen W, Wang L, Tan X, Yang D, Yuan J, Yang J. State-of-the-art and development tendency of the underground engineering stability of fractured rock mass. *Chinese J Rock Mech Eng*. 2021;10:945-1961. doi:10.13722/j.cnki.jrme.2020.1074
2. Zhang Y, Zou Y, Zhang Y, et al. Experimental study on characteristics and mechanisms of matrix pressure transmission near the fracture surface during post-fracturing shut-in in tight oil reservoirs. *J Pet Sci Eng*. 2022;219:111133. doi:10.1016/j.petrol.2022.111133

3. Guo P, Wang M, Dang G, Zhu T, Wang J, He M. Evaluation method of underground water storage space and thermal reservoir model in abandoned mine. *Rock Mech Bull*. 2023;2(2):100044. doi:10.1016/j.rockmb.2023.100044
4. Mehrabian A, Abousleiman YN. Gassmann equations and the constitutive relations for multiple-porosity and multiple-permeability poroelasticity with applications to oil and gas shale. *Int J Numer Anal Methods Geomech*. 2015;39(14):1547-1569. doi:10.1002/nag.2399
5. Shin HS, Kim KY, Pande GN. On computation of strain-dependent permeability of rocks and rock-like porous media. *Int J Numer Anal Methods Geomech*. 2015;39(8):821-832. doi:10.1002/nag.2334
6. Bagherzadeh P, Goshtasbi K, Kazemzadeh E, Kashef M, Aloki Bakhtiari H. Stress-dependence of the permeability, porosity, and compressibility in fractured porous media regarding fracturing condition. *Bull Eng Geol Environ*. 2021;80:5091-5110. doi:10.1007/s10064-021-02215-4
7. Hsieh PA, Tracy JV, Neuzil CE, Bredehoeft JD, Silliman SE. A transient laboratory method for determining the hydraulic properties of 'tight'rocks—I. Theory. *Int J Rock Mech Min Sci*. 1981;18(3):245-252. doi:10.1016/0148-9062(81)90979-7
8. Brace W, Walsh JB, Frangos WT. Permeability of granite under high pressure. *J Geophys Res*. 1968;73(6):2225-2236. doi:10.1029/JB073i006p02225
9. David C, Wong TF, Zhu W, Zhang J. Laboratory measurement of compaction-induced permeability change in porous rocks: implications for the generation and maintenance of pore pressure excess in the crust. *Pure Appl Geophys*. 1994;143(1-3):425-456. doi:10.1007/BF00874337
10. Dong JJ, Hsu JY, Wu WJ, et al. Stress-dependence of the permeability and porosity of sandstone and shale from TCDP Hole-A. *Int J Rock Mech Min Sci*. 2010;47(7):1141-1157. doi:10.1016/j.ijrmms.2010.06.019
11. Ghabezloo S, Sulem J, Guédon S, Martineau F. Effective stress law for the permeability of a limestone. *Int J Rock Mech Min Sci*. 2009;46(2):297-306. doi:10.1016/j.ijrmms.2008.05.006
12. Zimmerman RW. *The Effect of Pore Structure on the Pore and Bulk Compressibilities of Consolidated Sandstones*. PhD dissertation. University of California; 1984.
13. Watanabe T, Higuchi A. Simultaneous measurements of elastic wave velocities and electrical conductivity in a brine-saturated granitic rock under confining pressures and their implication for interpretation of geophysical observations. *Prog Earth Planet Sci*. 2015;2(1):2-37. doi:10.1016/10.1186/s40645-015-0067-0
14. Zhang C, Chen Y, Ren Z, Wang F. Compaction and seepage characteristics of broken coal and rock masses in coal mining: a review in laboratory tests. *Rock Mech Bull*. 2024;3(2):100102. doi:10.1016/j.rockmb.2024.100102
15. Chen D, Pan Z, Ye Z, Hou B, Wang D, Yuan L. A unified permeability and effective stress relationship for porous and fractured reservoir rocks. *J Nat Gas Sci Eng*. 2016;29:401-412. doi:10.1016/j.jngse.2016.01.034
16. Chen M, Masum S, Sadasivam S, Thomas H. Modelling anisotropic adsorption-induced coal swelling and stress-dependent anisotropic permeability. *Int J Rock Mech Min Sci*. 2022;153:105107. doi:10.1016/j.ijrmms.2022.105107
17. Civan F. Stress-dependent porosity and permeability of porous rocks represented by a mechanistic elastic cylindrical pore-shell model. *Transp Porous Media*. 2019;129(3):885-899. doi:10.1007/s11242-019-01311-0
18. Tan X, Chen W, Wang L, Yang J, Tan XJ. Settlement behaviors investigation for underwater tunnel considering the impacts of fractured medium and water pressure. *Mar Georesources Geotechnol*. 2021;39:639-648. doi:10.1080/1064119X.2020.1737279
19. Guo P, Cheng Y, Jin K, Li W, Tu Q, Liu H. Impact of effective stress and matrix deformation on the coal fracture permeability. *Transp Porous Media*. 2014;103(1):99-115. doi:10.1007/s11242-014-0289-4
20. Zhang R, Ning Z, Yang F, Zhao H, Wang Q. A laboratory study of the porosity-permeability relationships of shale and sandstone under effective stress. *Int J Rock Mech Min Sci*. 2016;81:19-27. doi:10.1016/j.ijrmms.2015.11.006
21. Gutierrez M, Katsuki D, Tutuncu A. Determination of the continuous stress-dependent permeability, compressibility and poroelasticity of shale. *Mar Pet Geol*. 2015;68:614-628. doi:10.1016/j.marpetgeo.2014.12.002
22. Bernabé, Y., Mok U, Evans B. Permeability-porosity relationships in rocks subjected to various evolution processes. *Pure Appl Geophys*. 2003;160:937-960. doi:10.1007/PL00012574
23. Zimmerman RW. *Compressibility of Sandstones*. Elsevier; 1991.
24. Kwon O, Kronenberg AK, Gangi AF, Johnson B. Permeability of Wilcox shale and its effective pressure law. *J Geophys Res Solid*. 2001;106(B9):19339-19353. doi:10.1029/2001JB000273
25. Mitchell TM, Faulkner DR. Experimental measurements of permeability evolution during triaxial compression of initially intact crystalline rocks and implications for fluid flow in fault zones. *J Geophys Res Solid*. 2008;113(B11):1-16. doi:10.1029/2008JB005588
26. Dietrich P, Helmig R, Sauter M, Teutsch G, Hötzl H, Köngeter J. *Flow and Transport in Fractured Porous Media*. Springer-Verlag; 2005. doi:10.1007/b138453
27. Wang L, Yin ZY, Han G, Yu M. Toward temporal evolution of consolidation in fluid-saturated poroelastic media with various permeable conditions. *Comput Geotech*. 2023;156:105273. doi:10.1016/j.compgeo.2023.105273
28. Liu HH, Rutqvist J, Berryman JG. On the relationship between stress and elastic strain for porous and fractured rock. *Int J Rock Mech Min Sci*. 2009;46:289-296. doi:10.1016/j.ijrmms.2008.04.005
29. Zheng J, Zheng L, Liu HH, Ju Y. Relationships between permeability, porosity and effective stress for low-permeability sedimentary rock. *Int J Rock Mech Min Sci*. 2015;78:304-318. doi:10.1016/j.ijrmms.2015.04.025
30. Ogden RW. *Non-Linear Elastic Deformations*. Dover Publications; 1997.
31. Belytschko T, Liu WK, Moran B, Elkhodary K. *Nonlinear finite elements for continua and structures*. John Wiley & Sons; 2014.
32. Li L, Liu HH, Birkholzer J, Vietor T. The use of two-part Hooke's model (TPHM) to model the mine-by test at Mont Terri Site, Switzerland. *Comput Geotech*. 2014;58:28-46. doi:10.1016/j.compgeo.2014.02.001

33. Ye Z, Yang J, Xiong F, Huang S, Cheng A. Analytical relationships between normal stress and fluid flow for single fractures based on the two-part Hooke's model. *J Hydro*. 2022;608:127633. doi:10.1016/j.jhydrol.2022.127633
34. Zhu QZ, Kondo D, Shao JF. Micromechanical analysis of coupling between anisotropic damage and friction in quasi brittle materials: role of the homogenization scheme. *Int J Solids Struct*. 2008;45(5):1385-1405. doi:10.1016/j.ijsolstr.2007.09.026
35. Wang L, Chen W, Vuik C. Hybrid-dimensional modeling for fluid flow in heterogeneous porous media using dual fracture-pore model with flux interaction of fracture-cavity network. *J Nat Gas Sci Eng*. 2022;100:104450. doi:10.1016/j.jngse.2022.104450
36. Wang L, Golfier F, Tinet AJ, Chen W, Vuik C. An efficient adaptive implicit scheme with equivalent continuum approach for two-phase flow in fractured Vuggy porous media. *Adv Water Resour*. 2022;163:104186. doi:10.1016/j.advwatres.2022.104186
37. Berryman JG. Effective-stress rules for pore-fluid transport in rocks containing two minerals. *Technical Note*. Lawrence Livermore National Laboratory; 1993.
38. Davies JP, Davies DK. Stress-dependent permeability: characterization and modeling. *SPE J*. 2001;6(02):224-235. doi:10.2118/71750-PA
39. Neuzil CE. Hydromechanical coupling in geologic processes. *Hydro J*. 2003;11:41-83. doi:10.1007/s10040-002-0230-8
40. Berryman JG. Modeling nonlinear response of fractured rocks and reservoirs. *Int J Numer Anal Methods Geomech*. 2017;41(5):771-780. doi:10.1002/nag.2656
41. Jaeger JC, Cook NG, Zimmerman R. *Fundamentals of Rock Mechanics*. John Wiley & Sons; 2009.
42. Chen Y, Wong TF, Liu ER. *Rock Physics*. University of Science and Technology of China Publishing House; 2009.
43. Green DH, Wang HF. Specific storage as a poroelastic coefficient. *Water Resour Res*. 1990;26(7):1631-1637. doi:10.1029/WR026i007p01631
44. Shi Y, Wang CY. Pore pressure generation in sedimentary basins: overloading versus aquathermal. *J Geophys Res Solid*. 1986;91(B2):2153-2162. doi:10.1029/JB091iB02p02153
45. Kim K, Makhnenko RY. Coupling between poromechanical behavior and fluid flow in tight rock. *Transp Porous Media*. 2020;135:487-512. doi:10.1007/s11242-020-01484-z
46. Tai PL, Nguyen XX, Dong JJ. A novel method to estimate the Stress-dependent Kozeny-Carman constant of low-permeability, clastic sedimentary rocks. *J Hydrol*. 2023;621:129595. doi:10.1016/j.jhydrol.2023.129595
47. Tan X, Chen W, Wang L, Ye W. Development of an optimization model for monitoring point in tunnel stress deduction using machine learning algorithm. *Deep Undergr Sci Eng*. 2024. (In press). doi:10.1002/dug2.12076
48. Tan X, Chen W, Wang L, Qin C. Spatial deduction of mining-induced stress redistribution using an optimized non-negative matrix factorization model. *J Rock Mech Geotech Eng*. 2023;15(11):2868-2876. doi:10.1016/j.jrmge.2022.12.008
49. Miranda LJ. PySwarms: a research toolkit for particle swarm optimization in Python. *J Open Source Softw*. 2018;3(21):433. doi:10.21105/joss.00433
50. Guest PG. *Numerical Methods of Curve Fitting*. Cambridge University Press; 2012.
51. Witherspoon PA, Wang JS, Iwai K, Gale JE. Validity of cubic law for fluid flow in a deformable rock fracture. *Water Resour Res*. 1980;16(6):1016-1024. doi:10.1029/WR016i006p01016
52. Al-Wardy W, Zimmerman RW. Effective stress law for the permeability of clay-rich sandstones. *J Geophys Res Solid*. 2004;109(B4):1-10. doi:10.1029/2003JB002836
53. Berryman JG. Effective stress for transport properties of inhomogeneous porous rock. *J Geophys Res Solid*. 1992;97(B12):17409-17424. doi:10.1029/92JB01593
54. Wang LY, Chen WZ, Zhang YJ, Zhang XD, Vuik C. Investigating effects of heterogeneity and fracture distribution on two-phase flow in fractured reservoir with adaptive time strategy. *Transp Porous Media*. 2023;149:175-203. doi:10.1007/s11242-022-01850-z
55. Wang L, Wang Y, Vuik C, Hajibeygi H. Accurate modeling and simulation of seepage in 3D heterogeneous fractured porous media with complex structures. *Comput Geotech*. 2022;150:104923. doi:10.1016/j.compgeo.2022.104923

How to cite this article: Wang L, Zhang Y. Interpreting correlations in stress-dependent permeability, porosity, and compressibility of rocks: A viewpoint from finite strain theory. *Int J Numer Anal Methods*. 2024;48:2000–2019. https://doi.org/10.1002/nag.3720